Journal of Materials Chemistry C

RSC Publishing

PAPER

View Article Online
View Journal | View Issue

Cite this: *J. Mater. Chem. C*, 2013, **1**, 7623

Novel programmable functional polyimides: preparation, mechanism of CT induced memory, and ambipolar electrochromic behavior†

Chih-Jung Chen,‡ Hung-Ju Yen,‡ Yi-Cheng Hu and Guey-Sheng Liou*

Received 14th August 2013
Accepted 19th September 2013

DOI: 10.1039/c3tc31598c

www.rsc.org/MaterialsC

In this study, the new functional polyimides **9Ph-ODPI**, **9Ph-DSPI**, and **9Ph-PMPI** consisting of electron-donating starburst triarylamine units and different dianhydrides were synthesized and used for memory device applications along with **9Ph-6FPI**. To investigate the effects of donor moieties in polyimides on their memory behavior, the corresponding **3Ph-** series polyimides (**3Ph-PIs**) and **5Ph-PIs** were also discussed. With the intensity of electron donation increasing from **3Ph-PIs** to **5Ph-PIs** to **9Ph-PIs**, the retention time of the memory device shows a systematic increase. The retention time of the memory device also increases with the increasing electron-withdrawing intensity of the dianhydrides. Furthermore, the *in situ* UV-vis absorption spectra of the memory devices during switching-ON were utilized as direct evidence to confirm the relationship between charge transfer (CT) complex stability and memory retention time. In electrochromic (EC) applications, the novel ambipolar **9Ph-PMPI** exhibited a high contrast ratio and electroactive stability during EC operation with multiple colors at different applied potentials, due to its four oxidation and two reduction states. Finally, flexible colorful EC and volatile memory devices were fabricated for practical flexible electronics applications in the future.

Introduction

In recent years, the use of polymeric materials in optoelectronic devices has attracted significant attention, such as light-emitting diodes,[1] transistors,[2] solar cells,[3] electrochromic (EC),[4] and memory devices,[5] resulting from the advantages of rich structural flexibility, low cost, solution processability, and three-dimensional stacking capability.[6] Among these applications, polymeric memory devices have been investigated as a promising alternative to the conventional semiconductor-based memory devices. Compared with conventional inorganic memory materials, polymeric memory materials store information in the form of high (ON) and low (OFF) current states, rather than the amount of charge stored in a cell of silicon devices, and have the added advantages of higher data storage density, ease of miniaturization, longer data retention time, fast speed, and low power consumption for practical use.[7] Thus, polymeric materials with electrical bistability resulting from a conductivity difference in response to an applied electric field begin to stand out as potential materials to face the problems and challenges in scaling down from the micro-scale to the nano-scale.

In the initial stages of polymer memory applications, polymers were used as polyelectrolytes and matrices in a doped system.[8] To advance the function of polymers for memory devices further, the design and synthesis of polymers with specific structures that can provide expected memory properties within a single polymer chain is an important issue. For resistive-type memory materials, electron donor–acceptor polymers are considered as suitable materials because charge transfer (CT) between the donor and acceptor moieties can give rise to a highly conductive state.[5a] There have been a number of demonstrations of the application of donor–acceptor polymers in memory device, such as conjugated polymers,[9] polymers with pendant electroactive chromophores,[10] functional polyimides,[11] and hybrid composites.[12] Among all the studied donor–acceptor systems, aromatic polyimides are promising candidates for memory device applications due to their excellent thermal dimensional stability, chemical resistance, mechanical strength, and high ON/OFF current ratio, resulting from the low conductivity in the OFF state. Although aromatic polyimides have superior properties, their applications are generally restricted by their limited solubility in most organic solvents and their high glass transition (T_g) or melting temperatures, caused by their high crystallinity, high stiffness of the polymer backbones, and CT complex formation. To overcome the solubility problem of polyimides, the non-coplanar triphenylamine

Functional Polymeric Materials Laboratory, Institute of Polymer Science and Engineering, National Taiwan University, 1 Roosevelt Road, 4th Sec., Taipei 10617, Taiwan. E-mail: gsliou@ntu.edu.tw

† Electronic supplementary information (ESI) available: IR spectra of **9Ph-DSPI**, TGA thermograms and UV-vis absorption spectra of **9Ph-PIs**, current–voltage (*I–V*) characteristics of **3Ph-PIs**, simulation results of **3Ph-PIs**, **5Ph-PIs**, and **9Ph-PIs**, electrochromic stability of **9Ph-PMPI**, and basic and thermal properties of **9Ph-PIs**. See DOI: 10.1039/c3tc31598c

‡ These authors contributed equally to this work.

(TPA) group was introduced into polyimides to enhance the solution processability. Furthermore, TPA could act as a donor to facilitate the CT behavior of polyimide, and therefore a series of TPA-based polyimides with different substituted groups were prepared for memory devices.[13] In our previous study,[13a] we demonstrated the effects of different dianhydrides (an electron acceptor) within the TPA-based polyimide backbone on memory properties. Polyimides with different electron-withdrawing intensity acceptors revealed anomalous properties, from dynamic random access memory (DRAM), static dynamic random access memory (SRAM) to write-once-read-many-times (WORM). However, the donor capability difference among the TPA-based polyimides with different substituted groups previously reported is not obvious,[13c,d] and has not been investigated systematically yet. Furthermore, among the discussed switching mechanisms of memory behavior, field induced CT is a well-known one and has been used to explain the resulting memory behavior to a great extent. However, it is hard to find conclusive evidence for such a CT-based switching mechanism. Kang *et al.* have measured the UV-vis spectroscopy before and after switching of a polymer memory device showing SRAM behavior and explained the formation of the CT complex,[13e] but the UV-vis absorption spectra could not be measured during the switching process and were not sufficient to prove such formation. Therefore, the *in situ* UV-vis absorption spectra during the switching of memory devices based on the new functional polyimides **9Ph-ODPI**, **9Ph-DSPI**, and **9Ph-PMPI** with different memory characteristics were investigated in this work to provide direct and striking evidence for the formation of the CT complex, and make the field induced CT theory a decisive one.

High-performance polymers (*e.g.*, polyimide and polyamide[5b]) containing electron-donating triarylamine moieties are favorable functional materials not only for memory devices, but also for EC applications.[14] Since 2005, our group has reported several TPA-containing anodic EC polymers with interesting color transitions,[14] which showed excellent electrochemical reversibility in the visible region and the NIR range. Recently, we reported the starburst triarylamine-based polyimide **9Ph-6FPI** for both polymeric volatile memory and multi-colored EC devices.[13h] By combining the electron-donating starburst triarylamine moiety with a methoxyl group at the *para*-position of phenyl groups, the coupling reaction between TPA units of the prepared polyimide could be greatly prevented by affording stable cationic radicals at a much lower oxidation potential (higher HOMO energy level).[16] Additionally, the polyimide **9Ph-6FPI** revealed four reversible oxidation states with high EC contrast ratio and outstanding stability for long-term operation. Furthermore, by the introduction of the more conjugated pyromellitic dianhydride (PMDA) into this starburst triarylamine-based polyimide, the resulting polyimide could be expected to show more color states due to the additional electrochromic behavior from reduction.

In this study, we therefore synthesized the new functional polyimides **9Ph-ODPI**, **9Ph-DSPI**, and **9Ph-PMPI** consisting of electron-donating *N*,*N*′-bis[4-(4-methoxyphenyl-4-aminophenylamino)phenyl]-*N*′,*N*′-di(4-methoxyphenyl)-*p*-phenylenediamine and different dianhydrides for memory device applications along with **9Ph-6FPI**. The corresponding **3Ph-**series polyimides (**3Ph-PIs**) and **5Ph-** series polyimides (**5Ph-PIs**) were also discussed to systematically investigate and demonstrate the effect of different electron-donating and electron-withdrawing moieties within the TPA-based polyimides on the memory behavior. Additionally, the *in situ* UV-vis absorption spectra of memory devices during switch-ON were utilized as direct evidence to confirm the relationship between CT complex stability and memory retention time. Furthermore, the EC behavior of **9Ph-PMPI** was investigated and was expected to reveal multiple colors at different applied potentials due to its four oxidation states and two reduction states. The flexible colorful EC and polymeric memory devices were further fabricated and investigated in this study.

Results and discussion

Synthesis and basic characterization of polyimides

The new starburst polyimides **9Ph-ODPI** and **9Ph-DSPI** were prepared by the reaction of diamine (**1**) with the commercially available dianhydrides oxydiphthalicanhydride (ODPA) (**2**) and 3,3′,4,4′-diphenylsulfonetetracarboxylic dianhydride (DSDA) (**4**) in *m*-cresol in the presence of isoquinoline by a one-step method (Scheme 1). **9Ph-PMPI** was prepared by the reaction of diamine (**1**) with the commercially available 1,2,4,5-benzenetetracarboxylic anhydride (PMDA) (**5**) in *N*-methyl-2-pyrrolidinone (NMP) at room temperature to form the precursor poly(amic acid), followed by chemical imidization. The synthesis and characterization of **9Ph-6FPI** has been described previously.[13h] The inherent viscosity and GPC analysis data of these **9Ph-**series polyimides (**9Ph-PIs**) are summarized in Table S1.† Polydispersity indices of 1.9–2.4 were measured for the molecular weight distribution, which are ideal values for polycondensations. The high molecular weights could afford good quality thin films *via* spin coating or solution casting for memory and electrochromic devices. The IR spectrum of **9Ph-DSPI** was used as an example to confirm polyimide formation, as shown in Fig. S1,† and exhibited characteristic imide absorption bands at 1781 (asymmetric C=O stretch), 1725 (symmetric C=O stretch), 1379 (C–N stretch), and 738 cm^{-1} (imide ring deformation).

The solubility properties of **9Ph-PIs** were investigated quantitatively and the results are listed in Table S2.† The **9Ph-PIs** were highly soluble not only in polar aprotic organic solvents such as NMP and *N*,*N*-dimethylacetamide (DMAc), but also in less polar solvents such as tetrahydrofuran (THF) and $CHCl_3$. Polyimides with anhydride PMDA usually exhibit poor solubility in common organic solvents, however, **9Ph-PMPI** has a certain degree of solubility in organic solvent, which could be attributed to the incorporation of bulky and three-dimensional starburst triarylamine moieties along the polymer backbone, resulting in large steric hindrance to close packing. Their excellent solubility makes these polymers good potential candidates for practical applications by spin coating or inkjet printing processes to afford high performance thin films for optoelectronic devices.

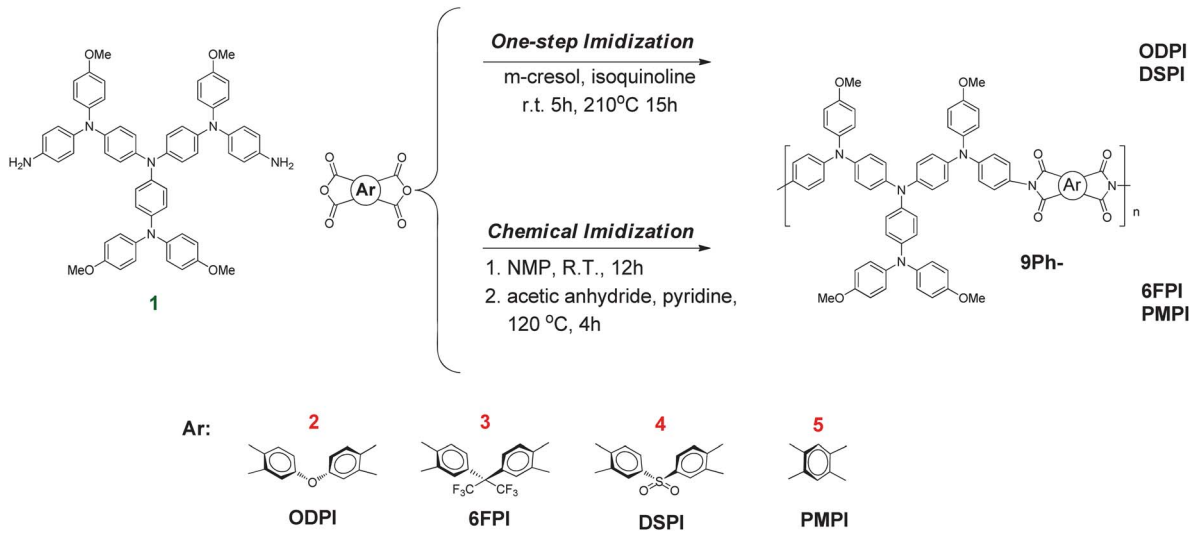

Scheme 1 Synthesis of novel **9Ph-** series polyimides by one-step imidization and chemical imidization.

The thermal properties of **9Ph-PIs** were examined by TGA and DSC, and the thermal behavior data are summarized in Table S3.† TGA curves of the polyimides are shown in Fig. S2.† The prepared polyimides exhibited good thermal stability with insignificant weight loss up to 350 °C, even with the introduction of methoxy groups. The carbonized residue (char yield) of these polymers in a nitrogen atmosphere was more than 59% at 800 °C, and the limiting oxygen indices were all above 41. The glass-transition temperatures (T_g) were in the range of 241–266 °C.

Absorption and electrochemistry

UV-vis absorption spectra of **9Ph-PIs** are depicted in Fig. S3,† and the onset wavelength of optical absorption was utilized to obtain the optical energy band gap (E_g) of the polyimides. The electrochemical properties of **9Ph-PIs** were investigated by cyclic voltammetry (CV), which was conducted by casting films on an indium–tin oxide (ITO)-coated glass slide as a working electrode in anhydrous acetonitrile (CH_3CN) or *N*,*N*-dimethylformamide (DMF), using 0.1 M of tetrabutylammonium perchlorate (TBAP) as a supporting electrolyte in a nitrogen atmosphere. The typical CV diagrams for **9Ph-PIs** are shown in Fig. 1, revealing four reversible oxidation redox couples originating from the diamine units and two reduction redox couples due to the aromatic-carbonyl π-system of the imide functional group for **9Ph-PMPI**, and one reduction redox couple for the other **9Ph-PIs**. The redox potentials of the polyimide as well as their respective highest occupied molecular orbital (HOMO) and lowest unoccupied molecular orbital (LUMO) (*versus* vacuum) were calculated and are summarized in Table 1. The onset oxidations of **9Ph-ODPI**, **9Ph-6FPI**, **9Ph-DSPI**, and **9Ph-PMPI** were found to be 0.34, 0.33, 0.34, and 0.35 V, respectively. The HOMO levels, or ionization potentials (*versus* vacuum), of the **9Ph-** polyimides could be estimated from the onset of their oxidation in CV experiments as 4.78, 4.77, 4.78 and 4.79 eV (on the basis that the ferrocene/ferrocenium couple is 4.8 eV below the vacuum level with $E_{onset} = 0.36$ V). The HOMO levels of the **9Ph-PIs** are similar and do not show obvious differences as they possess the same donor moiety. However, the LUMO levels calculated from the onset of their reduction potential are 3.45, 3.53, 3.56, and 3.68 eV, respectively. The LUMO energy levels of these polyimides decrease with the increasing electron-withdrawing capability of the dianhydride, in the order **9Ph-ODPI**, **9Ph-6FPI**, **9Ph-DSPI**, and **9Ph-PMPI**.

Memory device characteristics

The memory behaviors of these polyimides were examined by the current–voltage (*I*–*V*) characteristics of an ITO/polymer/Al sandwich device as shown in Fig. 2a. Within the sandwich device, a polymer film was used as an active layer between Al and ITO as the top and bottom electrodes. To exclude the effect of polymer film thickness on the memory properties, a standard

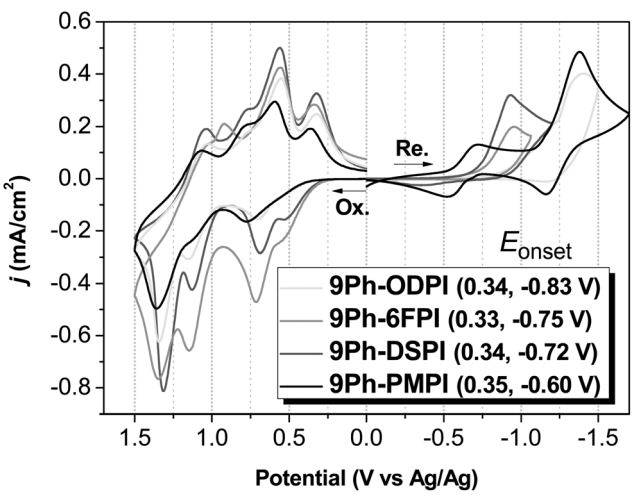

Fig. 1 Cyclic voltammetric diagrams of **9Ph-** series polyimides films on an ITO-coated glass substrate in 0.1 M TBAP acetonitrile (for the anodic process) and DMF (for the cathodic process) solution, at a scan rate of 50 mV s^{-1}.

Table 1 Redox potentials and energy levels of **9Ph-** series polyimides

Polymer	Thin films (nm) λ_{max}	Thin films (nm) λ_{onset}	Oxidation potential[a] (V) E_{onset}	Reduction potential[b] (V) E_{onset}	$E_g^{opt.c}$ (eV)	HOMO[d] (eV)	LUMO$^{Opt.e}$ (eV)	LUMO^{ECf} (eV)
9Ph-ODPI	332	537	0.34	−0.83	2.31	4.78	2.47	3.45
9Ph-6FPI	328	523	0.33	−0.75	2.37	4.77	2.40	3.53
9Ph-DSPI	322	559	0.34	−0.72	2.22	4.78	2.56	3.56
9Ph-PMPI	318	583	0.35	−0.60	2.13	4.79	2.66	3.68

[a] From cyclic voltammograms *vs.* Ag/AgCl in CH_3CN. [b] From cyclic voltammograms *vs.* Ag/AgCl in DMF. [c] The data were calculated from polymer films using the equation: $E_g = 1240/\lambda_{onset}$ (energy gap between HOMO and LUMO). [d] The HOMO energy levels were calculated from cyclic voltammetry and were referenced to ferrocene (4.8 eV; $E_{onset} = 0.36$ V in CH_3CN). [e] The LUMO energy levels were calculated from HOMO − E_g. [f] The LUMO energy levels were calculated from cyclic voltammetry and were referenced to ferrocene (4.8 eV; $E_{1/2} = 0.52$ V in DMF).

thickness (50 nm) was used unless otherwise specified. Fig. 3a shows the *I–V* results of **9Ph-ODPI**, which was measured with a compliance current of 0.01 A. During the first positive sweep from 0 V to 6 V, the device stayed in the low-conductivity (OFF) state with a current range of 10^{-12}–10^{-13} A, which means that the positive applied voltage could not switch the memory device on. On the other hand, the current increased abruptly from 10^{-12} to 10^{-13} to 10^{-4} A (the high-conductivity state) at the threshold voltage of −3.7 V in the second negative sweep, indicating the transition from the OFF state to the high-conductivity (ON) state. In a memory device, this OFF-to-ON transition can be defined as a "writing" process. The device remained in the ON state during the subsequent negative scan (the third sweep) and then positive scan (the fourth sweep). The memory device could not be reset to the initial OFF state by the application of a reverse scan, implying non-erasable behavior. The fifth sweep was conducted after turning off the power for about 15 seconds, and it was found that the ON state had relaxed to the steady OFF state. This suggests that the ON state could be retained for a short period of time after the removal of the applied voltage, before eventually relaxing to the initial OFF state. The device could also be reprogrammed by going from the OFF state to the ON state again with an accurate threshold voltage of −3.6 V in the fifth sweep, and remained in the ON state in the subsequent sixth sweep. The fifth and sixth sweeps were conducted to confirm that the memory device is re-writable. The very short retention time of the ON state indicates that the memory device of **9Ph-ODPI** showed volatile DRAM behaviour. Fig. 3b shows the *I–V* results of **9Ph-6FPI** showing SRAM behavior, which has been published previously.[13h]

Fig. 3c and d summarize the *I–V* results of **9Ph-DSPI** and **9Ph-PMPI**. During the second negative sweep from 0 V to −6 V, the current increased abruptly from 10^{-12} to 10^{-13} to 10^{-4} A at the threshold voltages of −4.1 V and −4.0 V, indicating the

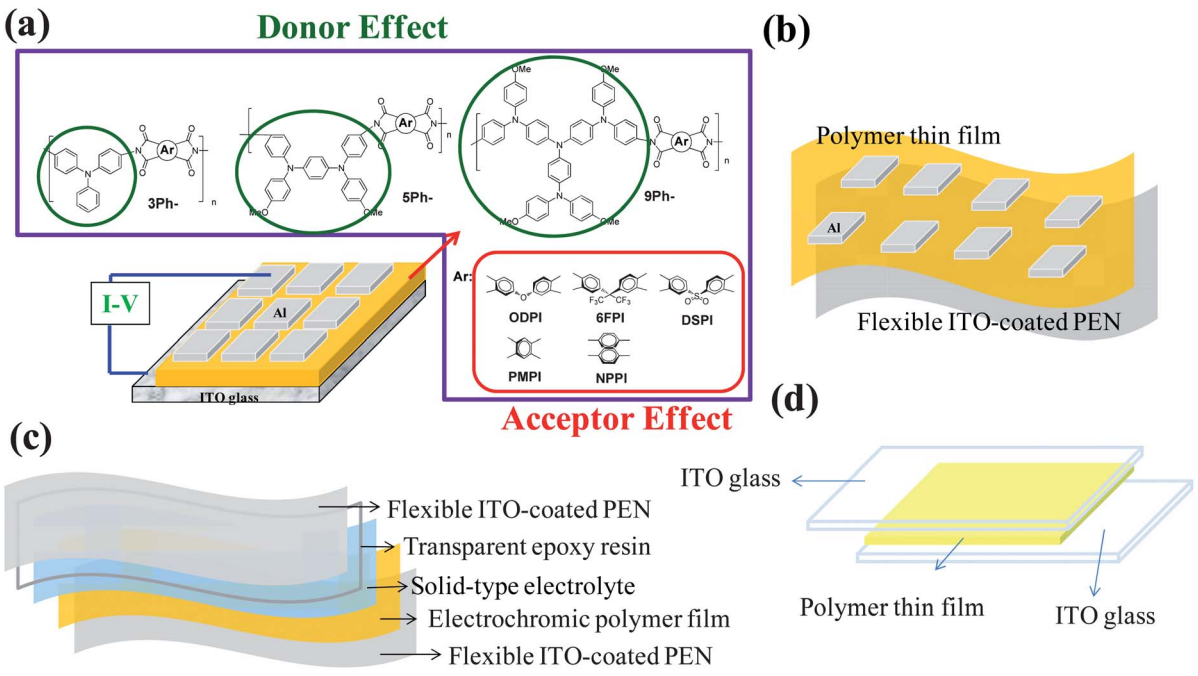

Fig. 2 (a) Molecular structures of polyimides and a schematic diagram of the memory device, (b) schematic diagram of a flexible memory device based on **9Ph-ODPI**, (c) configuration of the flexible electrochromic device based on **9Ph-PMPI**, and (d) the transparent memory device for "*in situ*" UV-vis absorption spectroscopy during switching-ON.

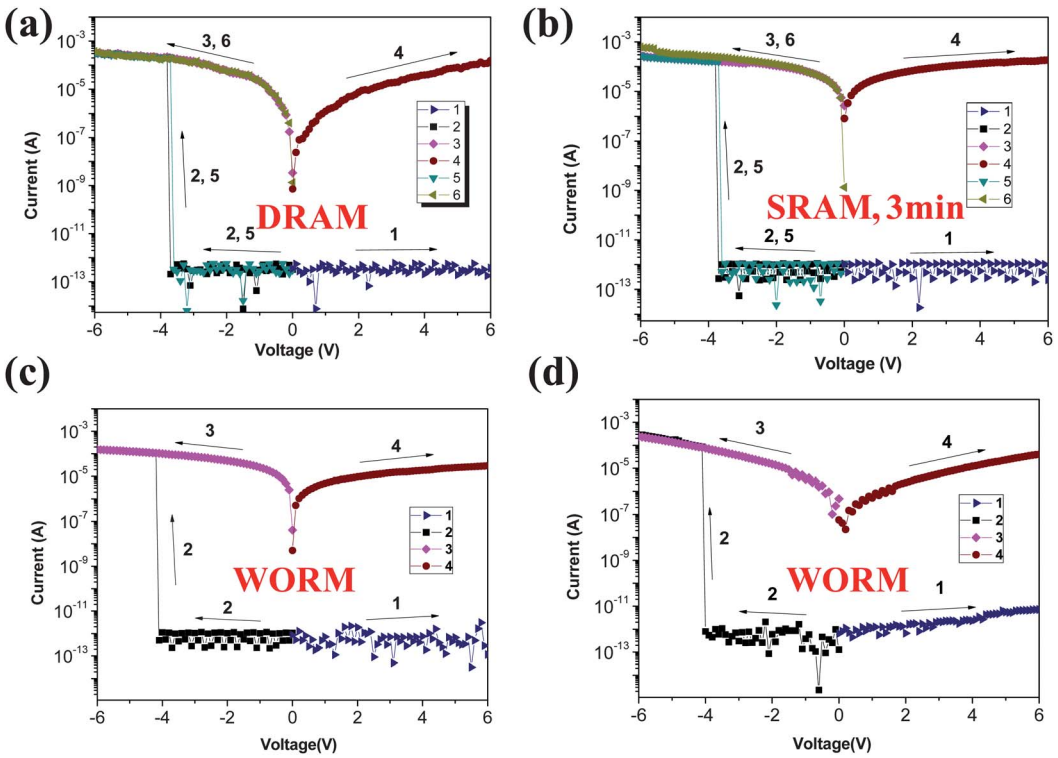

Fig. 3 Current–voltage (*I–V*) characteristics of the ITO/polyimide (50 ± 3 nm)/Al memory device. (a) **9Ph-ODPI**, (b) **9Ph-6FPI**, (c) **9Ph-DSPI**, (d) **9Ph-PMPI**.

transition from the OFF state to the ON state. The devices remained in the ON state during the subsequent negative scan (the third sweep) and then positive scan (the fourth sweep). Once the **9Ph-DSPI** and **9Ph-PMPI** memory devices have been switched to the ON state, the state was retained even after turning off the power for 1 hour or longer. These results indicate that the **9Ph-DSPI** and **9Ph-PMPI** films exhibit non-volatile WORM memory behavior in the device.

Fig. S4† depicts the *I–V* results of the **3Ph-PIs**. Different from **9Ph-ODPI**, the memory device of **3Ph-ODPI** remained in the OFF state during the positive and negative scan. Thus, **3Ph-ODPI** showed no memory, but showed insulator behavior. Compared to the **9Ph-PIs**, **3Ph-PIs** with the same dianhydride generally exhibited much shorter retention times, and the memory properties of **3Ph-PIs**, **5Ph-PIs**,[14] and **9Ph-PIs** are summarized in Fig. 4. As the electron-donating capability increased from **3Ph-PIs** to **5Ph-6FPI** to **9Ph-PIs**, the retention time of memory devices showed an increasing tendency. The retention time of the memory devices also increased with the increasing electron-withdrawing intensity of the dianhydrides. To obtain more insight into the memory behaviors of the polymeric devices, the molecular orbital and electric density contours of the basic units were estimated in detail by molecular simulations.

Switching mechanism

Molecular simulation of the basic units of the **9Ph-PIs** was carried out by DFT/B3LYP/6-31G(d) with the Gaussian 09 program.[15] The charge density isosurfaces of the basic unit, the most energetically favorable geometries, HOMO energy levels, LUMO energy levels, and dipole moments of the **9Ph-PIs** are depicted in Fig. 5. The LUMO energy levels calculated by molecular simulation could be utilized as evidence to indicate the electron-withdrawing capabilities of different dianhydrides. For these TPA-based polyimide systems, the HOMO energy levels were distributed mainly at the electron-donating TPA derivative moieties, while the LUMO energy levels were located at the electron-withdrawing phthalimide units. The simulation was also carried out for **3Ph-PIs** and the previously reported **5Ph-PIs**[14] for comparison, and the results were added to the discussion. Molecular simulation of the basic units of **3Ph-6FPI**, **5Ph-6FPI**, and **9Ph-6FPI** was chosen as an example to investigate and confirm the donor intensity, as shown in Fig. S5.† All the resulting HOMO energy levels, LUMO energy levels, and energy band gaps for **3Ph-PIs**, **5Ph-PIs**, and **9Ph-PIs** are summarized in Fig. S6.† The LUMO energy levels become lower with the increasing electron-withdrawing intensity of the

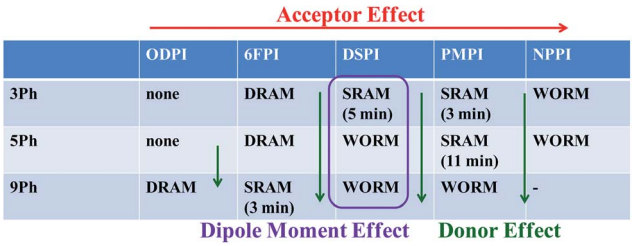

Fig. 4 Memory properties of **3Ph-PIs**, **5Ph-PIs**, and **9Ph-PIs**.

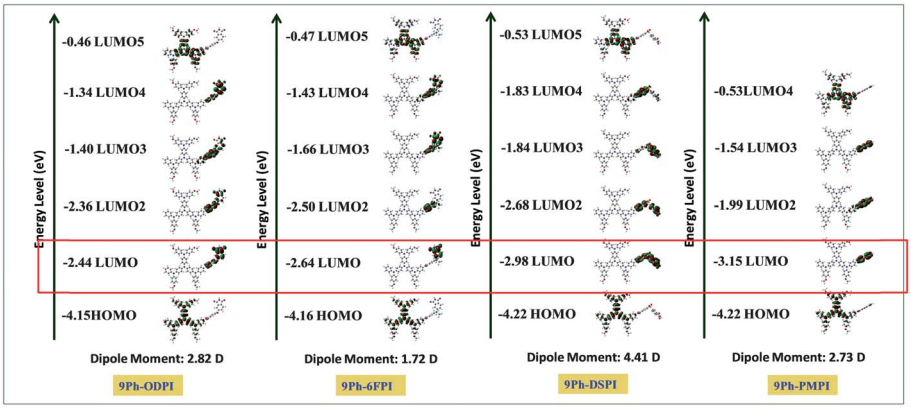

Fig. 5 Calculated molecular orbitals and corresponding energy levels of the basic units for **9Ph-** series polyimides.

dianhydrides among **9Ph-PIs**, which is in agreement with the reported literature.[13a] Also, the HOMO energy levels become higher with the increasing electron-donating capability from **3Ph-**, **5Ph-** to **9Ph-PIs**.

To explain the trends in memory properties, the stability of the CT complex was taken into consideration. According to the literature,[5a] when the applied electric fields reach the switching-on voltage, some electrons at the HOMO accumulate energy and transit to the LUMO5 (LUMO4 for **9Ph-PMPI**) with the highest probability, because of the overlapping of the HOMO and LUMO5, resulting in an excited state as shown in Fig. 5. Nevertheless, electrons at the HOMO may also be excited to the three intermediate LUMOs with lower energy barriers belonging to the acceptor units. Thus, CT occurs through several pathways to form the conductive CT complexes: indirectly from the LUMO5 through intermediate LUMOs and then to the LUMO, or from the intermediate LUMOs to the LUMO, or directly from the HOMO to the LUMO. When intra- or intermolecular CT occurred due to the applied electric field, the generated holes can be delocalized to the conjugated TPA derivative moieties, forming an open channel in the HOMO of polyimides for the charge carriers (holes) to migrate through. Therefore, the current increases rapidly and the memory device can be switched to the high conductivity state.

The LUMO energy level of polyimides is also a very important parameter for the retention time; because the CT complex is a metastable complex, lower LUMO values should make it more stable and allow it to exist for a longer time. Among the **9Ph-** series polyimides, **9Ph-ODPI** has the largest energy band gap and the weakest charge-transfer capability, which results in DRAM memory properties. Compared to the DRAM behavior of **9Ph-ODPI**, the lower LUMO energy level of **9Ph-6FPI** brings about a longer retention time, indicating SRAM characteristics. The lowest LUMO energy level and the strongest charge-transfer effect of **9Ph-DSPI** and **9Ph-PMPI** reveal non-volatile WORM behavior. In addition to the LUMO energy level, the value of the HOMO energy level also plays a crucial role in the stability of the CT complex. With the increasing electron-donating capability of TPA derivatives from **3Ph-** to **9Ph-** within the polyimides (higher HOMO energy levels), a more stable CT complex could be obtained and the retention time of memory devices increases. For example, the polyimides with the 6FDA dianhydride unit possess only DRAM properties for **3Ph-PIs** and **5Ph-PIs**, while they show SRAM behavior for **9Ph-PIs**. Thus, by the facile design of chemical structure, tunable memory properties with different retention times could be readily obtained. In addition to the acceptor and donor effect, the dipole moment of polyimides is also a critical factor for the retention time. Although **DSPI** has a higher LUMO energy level than **PMPI** among all the polyimide series, **DSPI** generally shows longer retention time than **PMPI**. The main difference between these two polyimides is the higher dipole moment of **DSPI**, which could stabilize the CT complex and results in memory properties with longer retention times.

Furthermore, "*in situ*" UV-vis absorption spectroscopy during the switching-ON of **9Ph-ODPI**, **9Ph-6FPI**, and **9Ph-DSPI** was utilized as direct evidence for field induced charge transfer memory behavior, and was carried out using transparent memory devices as shown in Fig. 2d. Fig. 6a depicts the UV-vis spectra of the **9Ph-ODPI** memory device before and after switching to the ON state, and the absorption changes after turning off the power. By switching the device from the OFF to the ON state, the intensity of the absorption peak at around 300–350 nm gradually increased, while this peak decreased in intensity after turning off the power for 10 seconds, and then recovered to the original state for only 15 seconds. This short retention time of the UV-vis absorption change after turning off the power was similar to the DRAM behavior of **9Ph-ODPI**. Compared to **9Ph-ODPI**, the absorption peak of **9Ph-6FPI** slowly decreased in intensity, and could also recover the original OFF state after turning off the device for 3 minutes, as shown in Fig. 6b. The same measurement of **9Ph-DSPI** is shown in Fig. 6c, but the absorption peak did not return to the original absorption OFF state even after turning off the device for 60 minutes. However, the absorption peak could be restored to the original off state by thermal treatment at around the T_g temperature, and was in good agreement with non-volatile WORM memory behavior. These "*in situ*" UV-vis absorption spectra measurements provide direct and solid evidence for the formation of the CT complex, and make the field induced CT theory an acceptable mechanism.

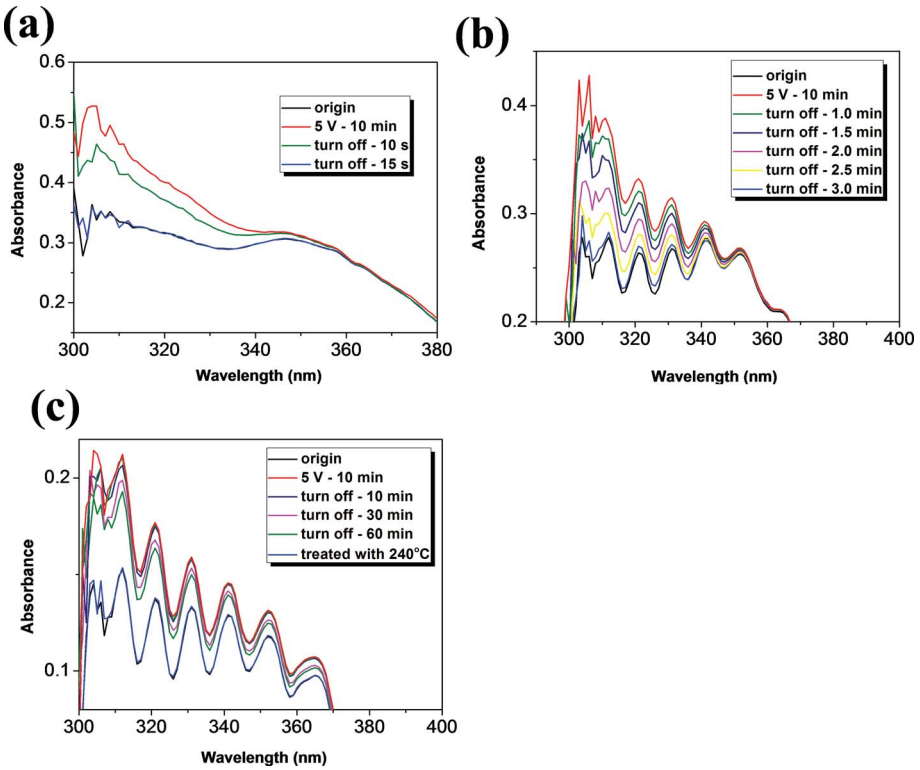

Fig. 6 *In situ* UV-visible spectra of the polymer memory devices of ITO/polyimide thin films/ITO during switch-ON: (a) **9Ph-ODPI**, (b) **9Ph-6FPI**, (c) **9Ph-DSPI**.

Spectroelectrochemical and electrochromic properties

Spectroelectrochemical experiments were used to evaluate the optical properties of the **9Ph-PMPI** EC films. For the investigation, a homemade electrochemical cell was built from a commercial UV-vis cuvette. The cell was placed in the optical path of the sample light beam in a UV-vis-NIR spectrophotometer, which allowed us to acquire electronic absorption spectra under potential control. UV-vis-NIR absorbance curves correlated to the electrode potentials of polyimide **9Ph-PMPI** are presented in Fig. 7, and were highly reversible and associated with strong color changes.

In the neutral form (0 V), the film exhibited strong absorption at around 352 nm, characteristic of triarylamine, but it was almost transparent in the visible region. Upon oxidation (increasing the applied voltage from 0 to 0.60 V), the intensity of the absorption peak at 352 nm gradually decreased while a new peak at 444 nm and a broad IV-CT band centered at around 1100 nm in the NIR region gradually increased in intensity. The first oxidation reversibility was 99%, based on the absorbance at 352 nm.[17a] We attribute the spectral change in the visible light range to the formation of a stable monocation radical **9Ph-PMPI**$^{+}$ in the TPA center of the starburst triarylamine moiety. Furthermore, the broad absorption in the NIR region is characteristic of IV-CT excitation between states in which the positive charge is centered at different nitrogen atoms, and is consistent with the phenomenon classified by Robin and Day.[17b] Meanwhile, the color of the film changed from colorless (L^*: 95; a^*: −3; b^*: 2) to yellow (L^*: 80; a^*: −13; b^*: 70). As the more anodic potential was increased to 0.90 V during the second oxidation stage, corresponding to **9Ph-PMPI**$^{2+}$, the absorption bands (352 and 444 nm) decreased gradually with new broad bands centered at around 555 and 1010 nm appearing, and the film became a purple color (L^*: 65; a^*: 8; b^*: −26) with a reversibility of 98%. By further applying a positive potential value up to 1.25 V, corresponding to **9Ph-PMPI**$^{3+}$, the characteristic absorbance at 608 and 804 nm appeared, and the strong IV-CT band at 1000 nm in the NIR region could still be observed with a lower reversibility of 78%. As shown in Fig. 7, the polymer film turned to a deep blue color (L^*: 45; a^*: 10; b^*: −28). When the applied potential was increased to 1.50 V, the absorption band at 1000 nm decreased gradually, with the appearance of a new broad band centered at around 735 nm, but only 55% absorbance remained, implying that the oxidation product (tetracation) was not stable. In the final stage, the absorption band can be attributable to the further oxidation of the **9Ph-PMPI**$^{3+}$ species to **9Ph-PMPI**$^{4+}$ in the starburst triarylamine segments, and the polymer film turned to a bluish-green color (L^*: 45; a^*: −18; b^*: −6).

The radical anion **9Ph-PMPI**$^{-}$, which appears at potentials between −0.90 and −1.50 V *vs.* Ag/AgCl, exhibits a strong band at 352 nm and two peaks in the visible region (stronger bands at 560 and 721 nm, with a shoulder at 657 nm). As shown in Fig. 7, the radical anion form of polyimide **9Ph-PMPI** is pale pink (L^*: 68; a^*: 20; b^*: 8) in color. The spectrum at −1.50 V (Fig. 7) has a strongly intensified peak at 560 nm with a concurrent drop of the absorption intensity at 657 and 721 nm, and the film turns to a red-violet color (L^*: 50; a^*: 27; b^*: 19) during the second reduction (dianion). The spectral changes associated with the reduction reactions of the pyromellitimide unit are very similar

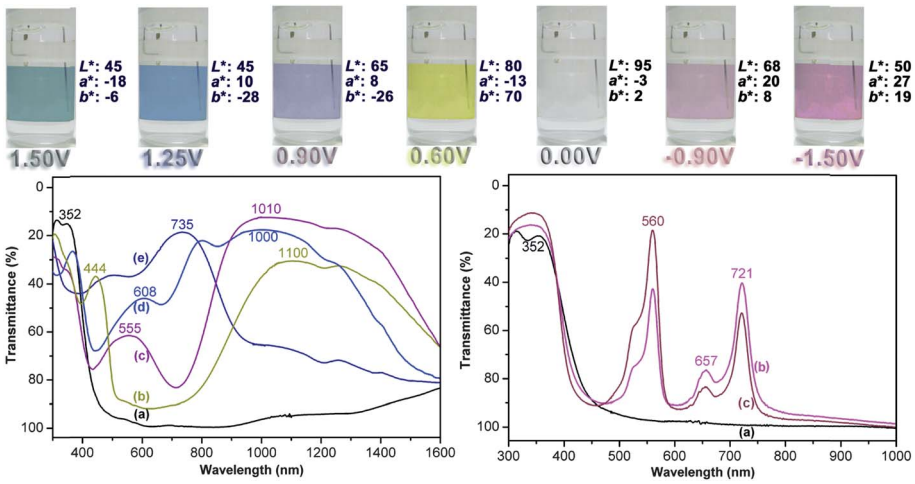

Fig. 7 EC behavior at applied potentials of (left) (a) 0.00, (b) 0.60, (c) 0.90, (d) 1.25, (e) 1.50, and (right) (a) 0.00, (b) −0.90, (c) −1.50 (V *vs.* Ag/AgCl) of polyimide **9Ph-PMPI** thin film (130 ± 10 nm thickness) on the ITO-coated glass substrate.

to that of PMDA-ODA polyimide (ODA: 4,4′-oxydianiline) reported by Mazur *et al.*[17c]

The film colorations are distributed homogeneously across the polymer film and reveal excellent stability for several thousands of redox cycles. The polyimide **9Ph-PMPI** shows good contrast both in the visible and NIR regions, with an extremely high optical transmittance change ($\Delta\%T$) of 82% at 1010 nm for purple coloring at the second oxidation stage, and 80% at 735 nm for the bluish-green coloring at the fourth oxidation stage. Because of the apparent high EC contrast, optical switching studies were investigated more deeply to examine the outstanding EC characteristics of the ambipolar multi-EC material.

Electrochromic switching studies

For the EC switching studies, polymer films were cast onto ITO-coated glass slides in the same manner as described above, and chronoamperometric and absorbance measurements were performed. While the films were switched, the absorbance at a given wavelength was monitored as a function of time by UV-vis-NIR spectroscopy. Switching data for the representative cast film of polyimide **9Ph-PMPI** are shown in Fig. S7 and S8.† The switching time was calculated at 90% of the full switch, because it is difficult to perceive any further color change with the naked eye beyond this point. As depicted in Fig. S7a,† when the potential was switched between 0 and 0.60 V, the polyimide **9Ph-PMPI** thin film revealed a switching time of 3.99 s for the coloring process and 0.90 s for bleaching. When the switched potential was set between 0 and 0.90 V, the **9Ph-PMPI** thin film required 3.12 s for coloration and 1.74 s for bleaching (Fig. S7b†). The polyimide switched rapidly between the highly transmissive neutral state and the colored oxidized states. The amount of injected/ejected charge (Q) was calculated from the integration of the current density and time obtained from Fig. S7c† to be 2.248 mC cm^{-2} and 2.245 mC cm^{-2} for oxidation and reduction processes at the first oxidation stage, respectively. The ratio of the charge density was 99.9%, indicating that charge injection/ejection was highly reversible during the electrochemical reactions. As shown in Fig. S8,† the EC stability of the polyimide **9Ph-PMPI** film was determined by measuring the optical change as a function of the number of switching cycles. The EC film of **9Ph-PMPI** was found to exhibit a high Coloration Efficiency (CE) ($\eta = \delta OD/Q$) up to 226 cm^2 C^{-1} at 1100 nm and 280 cm^2 C^{-1} at 1010 nm for the first and second oxidized states, respectively, exhibiting no decay of its electroactivity after 1000 cycles (Fig. S8†).

Flexible memory and electrochromic devices

To confirm the feasibility of the switching performance of the flexible memory devices, the device based on polyimide **9Ph-ODPI** was further characterized by physically fixing with a vernier caliper from flat to bent conditions (Fig. 8a). The memory device was tested under severe bending at various curvature radii of 11, 9, 7, and 5 mm, and the flexible device did not crack or deform upon bending. Reliable and reproducible switching memory behavior of the flexible device (Fig. 8b) also could be obtained under mechanical bending stress. Furthermore, we also fabricated single layer flexible EC cells based on polyimide **9Ph-PMPI** for long-term stability and bending investigations (Fig. S9†). The polymer film is colorless in the neutral form. When the voltage was increased consecutively (to a maximum of 2.0 V), the color changed to yellow, purple, blue, and then to bluish-green during different oxidation stages, as already observed in the spectroelectrochemical experiments. The polymer film could be subsequently turned back to the original colorless state when the potential was set back at 0 V. During the long-term stability measurements, with 10 hours for each coloring stage at applied potentials of 0.60 and 0.90 V, extremely high EC stability was observed, which reinforces and affords positive proof of the potential of the NIR electroactive aromatic polyimide for commercial applications. Considering the retained contrast ratio and electroactive stability during the EC operation, the novel polyimide shows the highest EC stability of any reported EC polymers, to the best of our

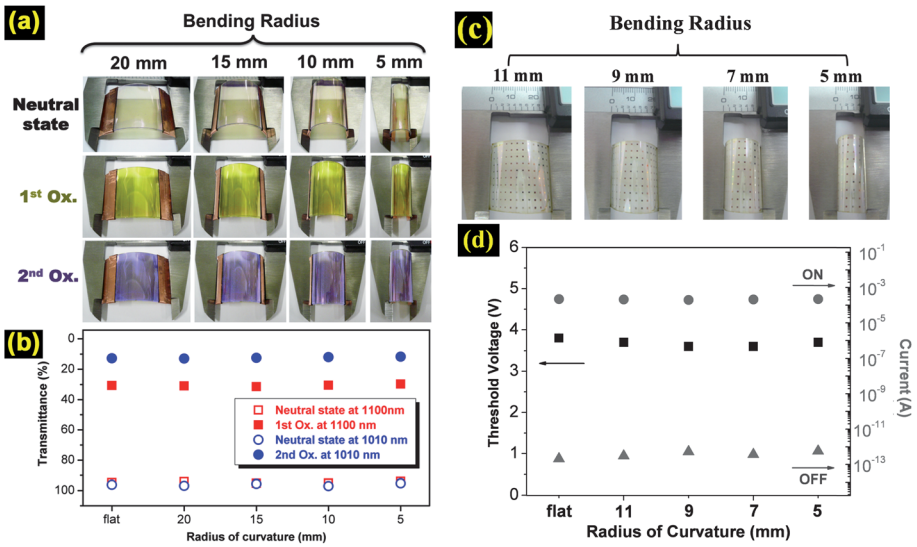

Fig. 8 (a) The single-layer flexible ITO-coated PEN EC device using polyimide **9Ph-PMPI** (130 ± 10 nm thickness) as the active layer in various bending and oxidative states. (b) Variation in transmittance of the flexible EC **9Ph-PMPI** device with different bending radii at the first and second oxidation stages. (c) Appearance of the flexible **9Ph-ODPI** memory device in various bent states. (d) Variation of current and threshold voltage with different bending radii of the ITO/**9Ph-ODPI** (50 ± 3 nm)/Al flexible memory device.

knowledge.[4] We believe that optimization could further improve the device performance and fully explore the potential of the EC polyimide. The flexible EC device was also characterized by physically fixing it in the same manner as described above (Fig. 8c). The transmittance responses of the flexible memory device at various bending radii were analyzed in detail and are shown in Fig. 8d, which suggests good flexibility and mechanical endurance. Severe bending of the EC device at various curvature radii of 20, 15, 10, and 5 mm did not degrade the device behavior, revealing that the flexible EC device is reliable even when the substrate is severely bent. The flexible multi-colored EC and memory devices are believed to have potential for practical flexible electronics applications in the future.

Conclusions

Three series of functional polyimides, **3Ph-PIs**, **5Ph-PIs**, and **9Ph-PIs**, consisting of electron-donating triarylamine units, were synthesized and used for memory devices. As the electron-donating capability increased from **3Ph-PIs** to **5Ph-PIs** to **9Ph-PIs**, the retention time of the resulting memory device shows an increasing trend. Additionally, the retention time of the memory device also increases with the increasing electron-withdrawing intensity of the dianhydrides. Furthermore, we clearly demonstrate the charge transfer induced memory mechanism by *in situ* UV-visible spectroscopy of polymer memory devices with DRAM, SRAM, and WORM behavior during switch-ON. For electrochromic (EC) applications, **9Ph-PMPI** not only revealed a high contrast ratio and retained its electroactive stability during long-term EC operation, but also exhibited multiple colors at different applied potentials due to its four oxidation and two reduction states. Finally, flexible ambipolar EC and memory devices could also be fabricated for practical flexible electronics applications in the future.

Experimental

Materials

N,*N*′-Bis[4-(4-methoxyphenyl-4-aminophenylamino)phenyl]-*N*′,*N*′-di(4-methoxyphenyl)-*p*-phenylenediamine (**1**) was synthesized according to a previously reported procedure.[4b] 2,2-Bis(3,4-dicarboxyphenyl)hexafluoropropane dianhydride (6FDA) (**2**) (Chriskev) was purified by vacuum sublimation. Oxydiphthalicanhydride (ODPA) (**3**) (Chriskev), 3,3′,4,4′-diphenylsulfonetetracarboxylic dianhydride (DSDA) (**4**) (TCI), and 1,2,4,5-benzenetetracarboxylic anhydride (PMDA) (**5**) (Chriskev) were purified by recrystallization from acetic anhydride. **9Ph-6FPI** was prepared according to the literature.[13h] Tetrabutylammonium perchlorate (TBAP) (Acros) was recrystallized twice from ethyl acetate in a nitrogen atmosphere and then dried *in vacuo* prior to use. All other reagents were used as received from commercial sources.

Polymer synthesis (one-step imidization)

The synthesis of polyimide **9Ph-DSPI** is used as an example to illustrate the general synthetic route for **9Ph-ODPI** and **9Ph-DSPI**. A stoichiometric mixture of diamine (**1**) (0.82 mmol) and dianhydride DSDA (**4**) (0.82 mmol, 0.36 g) in 3.1 mL of *m*-cresol was stirred at room temperature under nitrogen in the presence of a catalytic amount of isoquinoline. After the solution was stirred for 5 h, it was heated to 200 °C for 15 h, and the water produced by imidization was removed along with *m*-cresol. The obtained polymer solution was poured slowly into 300 mL of stirred methanol, giving rise to a fibrous precipitate that was collected by filtration, washed thoroughly with methanol, and dried under vacuum at 100 °C. Reprecipitations of the polymer from DMAc/methanol were carried out for further purification. The inherent viscosity and weight-average molecular weight (M_w) of the obtained polyimide were 0.31 dL g^{-1} (measured at a

concentration of 0.5 g dL^{-1} in DMAc at 30 °C) and 148 300 daltons, respectively. The FT-IR spectrum exhibited characteristic imide absorption bands at 1781 (asymmetric C═O stretch), 1725 (symmetric C═O stretch), 1379 (C–N stretch), and 738 cm^{-1} (imide ring deformation).

Polymer synthesis (chemical imidization)

To a solution of 0.47 g (0.53 mmol) of diamine (**1**) in 5.0 mL of NMP was added 0.12 g (0.53 mmol) of dianhydride PMDA (**5**) in one portion. The mixture was stirred at room temperature overnight (*ca*. 12 h) to afford a viscous poly(amic acid) solution. The poly(amic acid) was subsequently converted to polyimide **9Ph-PMPI** *via* a chemical imidization process by the addition of 1 mL pyridine and 2 mL acetic anhydride, and then the mixture was heated at 120 °C for 4 h to effect complete imidization. The obtained polymer solution was poured slowly into 300 mL of stirred methanol, giving rise to a stringy and fiber-like precipitate that was collected by filtration, washed thoroughly with methanol, and dried under vacuum at 100 °C. Reprecipitation of the polymer from NMP/methanol was carried out twice for further purification. The inherent viscosity and weight-average molecular weight (M_w) of the obtained polyimide were 0.30 dL g^{-1} (measured at a concentration of 0.5 g dL^{-1} in H_2SO_4 at 30 °C) and 135 400 daltons, respectively.

Fabrication of the flexible memory device

The memory device was fabricated with the configuration ITO coated PEN/polyimide/Al, as shown in Fig. 2b. The ITO coated poly(ethylene 2,6-naphthalate) (PEN) used for the memory device was cleaned by ultrasonication with water, acetone, and isopropanol for 15 min each. A 250 μl DMAc solution of polyimide (20–25 mg ml^{-1}) was first filtered through a 0.45 μm pore size PTFE membrane syringe filter, and then the filtered solution was spin-coated onto the ITO coated PEN at a rotation rate of 1000 rpm for 60 s and heated at 100 °C for 10 min under nitrogen. The film thickness was determined and controlled at around 50 nm. Finally, a 300 nm thick Al top electrode was thermally evaporated through the shadow mask (recorded device units of 0.5 × 0.5 mm^2 in size) at a pressure of 10^{-7} torr with a deposition rate of 3–6 Å s^{-1}.

Fabrication of the flexible electrochromic device

The electrochromic polymer film was prepared by coating a solution of the polyimide **9Ph-PMPI** (50 mg mL^{-1} in DMAc) onto an ITO coated PEN (20 mm × 30 mm × 0.3 mm, 20–30 Ω $\square^{-1}$), as depicted in Fig. 2c. The polymer was spin-coated onto the active area (20 mm × 20 mm) and then dried in a vacuum. A gel electrolyte based on poly(methyl methacrylate) (PMMA) (M_w: 350 000) and $LiClO_4$ was plasticized with propylene carbonate (5 g) to form a highly transparent and conductive gel. PMMA (3 g) was dissolved in dry acetonitrile (15 g), and $LiClO_4$ (0.3 g) was added to the polymer solution as a supporting electrolyte. The gel electrolyte was spread onto the polymer-coated side of the electrode, and the electrodes were sandwiched. Finally, an epoxy resin was used to seal the device.

Fabrication of the transparent memory device for *in situ* UV-visible absorption spectra during switching-ON

The device diagram is shown in Fig. 2d. Polymer memory thin film was prepared by coating a solution of the polyimide (25 mg mL^{-1} in DMAc) onto an ITO coated glass (20 mm × 30 mm × 0.3 mm). The polymer was spin-coated onto the active area (20 mm × 20 mm), then dried in a vacuum. After attaching another transparent ITO glass as the top electrode, the device was treated at 350 °C (above T_g) for 1 h to ensure a good adhesion between the polymer and the ITO glass before measurement.

Measurements

Fourier transform infrared (FT-IR) spectra were recorded on a PerkinElmer Spectrum 100 Model FT-IR spectrometer. The inherent viscosities were determined at 0.5 g dL^{-1} concentration using a Tamson TV-2000 viscometer at 30 °C. Gel permeation chromatographic (GPC) analysis was carried out on a Waters chromatography unit interfaced with a Waters 2410 refractive index detector at 3 mg mL^{-1} concentration. Two Waters 5 μm Styragel HR-2 and HR-4 columns (7.8 mm I. D. × 300 mm) were connected in series with NMP as the eluent at a flow rate of 0.5 mL min^{-1} at 40 °C and were calibrated with polystyrene standards. Thermogravimetric analysis (TGA) was conducted with TA SDT Q600. Experiments were carried out on approximately 6–8 mg film samples heated in flowing nitrogen or air (flow rate = 20 cm^3 min^{-1}) at a heating rate of 20 °C min^{-1}. Differential scanning calorimetry (DSC) analysis was performed on a PerkinElmer Pyris 1 DSC at a scan rate of 10 °C min^{-1} in flowing nitrogen (20 cm^3 min^{-1}). Electrochemistry was performed with a CH Instruments 611B electrochemical analyzer. Voltammograms are presented with the positive potential to the left and with increasing anodic currents pointing downwards. Cyclic voltammetry (CV) was conducted using a three-electrode cell in which ITO (polymer film area of about 0.5 cm × 1.2 cm) was used as a working electrode. A platinum wire was used as an auxiliary electrode. All cell potentials were taken using a homemade Ag/AgCl, KCl (sat.) reference electrode. Spectroelectrochemical experiments were carried out in a cell built from a 1 cm commercial UV-visible cuvette using a Hewlett-Packard 8453 UV-Visible diode array and a Hitachi U-4100 UV-vis-NIR spectrophotometer. The ITO-coated glass slide was used as the working electrode, a platinum wire as the counter electrode, and a Ag/AgCl cell as the reference electrode. CE (η) determines the amount of optical density change (δOD) at a specific absorption wavelength induced as a function of the injected/ejected charge (Q), which is determined from the *in situ* experiments. CE is given by the equation: $\eta = \delta OD/Q = \log[T_b/T_c]/Q$, where η (cm^2 C^{-1}) is the coloration efficiency at a given wavelength, and T_b and T_c are the bleached and colored transmittance values, respectively. The thickness of the polyimide thin film was measured with an alpha-step profilometer (Kosaka Lab, Surfcorder ET3000, Japan). Colorimetric measurements were obtained using a JASCO V-650 spectrophotometer, and the results are expressed in terms of lightness (L^*) and color coordinates (a^*, b^*). The electrical

characterization of the memory device was performed with a Keithley 4200-SCS semiconductor parameter analyzer equipped with a Keithely 4205-PG2 arbitrary waveform pulse generator. ITO was used as a common electrode and Al was the electrode for applying voltage during the sweep. The probe tip of a tinned copper shaft with a point radius of <0.1 μm was attached to a 10 μm diameter tungsten wire (GGB Industries, Inc.). The Gaussian 09 program package was used for theoretical calculation in this research, and the basic units were optimized by means of the density functional theory (DFT) method at the B3LYP level of theory (Beckesstyle three-parameter density functional theory using the Lee–Yang–Parr correlation functional) with the 6-31G(d) basis set.

Acknowledgements

We gratefully acknowledge the financial support of this research through the National Science Council of Taiwan.

References and Notes

1 (*a*) R. H. Friend, R. W. Gymer, A. B. Holmes, J. H. Burroughes, R. N. Marks, C. Taliani, D. D. C. Bradley, D. A. Dos Santos, J. L. Bredas, M. Logdlund and W. R. Salaneck, *Nature*, 1999, **397**, 121–128; (*b*) Q. Peng, E. T. Kang, K. G. Neoh, D. Xiao and D. Zou, *J. Mater. Chem.*, 2006, **16**, 376–383; (*c*) Y. Shao, X. Gong, A. J. Heeger, M. Liu and A. K. Y. Jen, *Adv. Mater.*, 2009, **21**, 1972–1975.

2 (*a*) H. Yan, Z. H. Chen, Y. Zheng, C. Newman, J. R. Quinn, F. Dotz, M. Kastler and A. Facchetti, *Nature*, 2009, **457**, 679–686; (*b*) Y. H. Chou, H. J. Yen, C. L. Tsai, W. Y. Lee, G. S. Liou and W. C. Chen, *J. Mater. Chem. C*, 2013, **1**, 3235–3243.

3 (*a*) G. Yu, J. Gao, J. C. Hummelen, F. Wudl and A. J. Heeger, *Science*, 1995, **270**, 1789–1791; (*b*) C. J. Brabec, N. S. Sariciftci and J. C. Hummelen, *Adv. Funct. Mater.*, 2001, **11**, 15–26; (*c*) M. H. Chen, J. Hou, Z. Hong, G. Yang, S. Sista, L. M. Chen and Y. Yang, *Adv. Mater.*, 2009, **21**, 4238–4242.

4 (*a*) H. J. Yen and G. S. Liou, *Chem. Mater.*, 2009, **21**, 4062–4070; (*b*) H. J. Yen, H. Y. Lin and G. S. Liou, *Chem. Mater.*, 2011, **23**, 1874–1882; (*c*) H. J. Yen and G. S. Liou, *Polym. Chem.*, 2012, **3**, 255–264; (*d*) S. V. Vasilyeva, P. M. Beaujuge, S. J. Wang, J. E. Babiarz, V. W. Ballarotto and J. R. Reynolds, *ACS Appl. Mater. Interfaces*, 2011, **3**, 1022–1032; (*e*) E. Puodziukynaite, J. L. Oberst, A. L. Dyer and J. R. Reynolds, *J. Am. Chem. Soc.*, 2012, **134**, 968–978; (*f*) E. P. Knott, M. R. Craig, D. Y. Liu, J. E. Babiarz, A. L. Dyer and J. R. Reynolds, *J. Mater. Chem.*, 2012, **22**, 4953–4962; (*g*) P. M. Beaujuge, S. V. Vasilyeva, D. Y. Liu, S. Ellinger, T. D. McCarley and J. R. Reynolds, *Chem. Mater.*, 2012, **24**, 255–268.

5 (*a*) Q. D. Ling, F. C. Chang, Y. Song, C. X. Zhu, D. J. Liaw, D. S. H. Chan, E. T. Kang and K. G. Neoh, *J. Am. Chem. Soc.*, 2006, **128**, 8732–8733; (*b*) C. J. Chen, H. J. Yen, W. C. Chen and G. S. Liou, *J. Polym. Sci., Part A: Polym. Chem.*, 2011, **49**, 3709–3718; (*c*) Y. Li, Y. Chu, R. Fang, S. Ding, Y. Wang, Y. Shen and A. Zheng, *Polymer*, 2012, **53**, 229–240; (*d*) B. L. Hu, F. Zhuge, X. J. Zhu, S. S. Peng, X. X. Chen, L. Pan, Q. Yan and R. W. Li, *J. Mater. Chem.*, 2012, **22**, 520–526; (*e*) Y. C. Hu, C. J. Chen, H. J. Yen, K. Y. Lin, J. M. Yeh, W. C. Chen and G. S. Liou, *J. Mater. Chem.*, 2012, **22**, 20394–20402; (*f*) T. Kurosawa, T. Higashihara and M. Ueda, *Polym. Chem.*, 2013, **4**, 16–30.

6 A. Stikeman, *Technol. Rev.*, 2002, 31.

7 (*a*) H. Gruber, *Res. Policy*, 2000, **29**, 725–740; (*b*) S. Moller, C. Perlov, W. Jackson, C. Taussig and S. R. Forrest, *Nature*, 2003, **426**, 166–169.

8 (*a*) B. Cho, T. W. Kim, S. Song, Y. Ji, M. Jo, H. Hwang, G. Y. Jung and T. Lee, *Adv. Mater.*, 2010, **22**, 1228–1232; (*b*) T. W. Kim, D. F. Zeigler, O. Acton, H. L. Yip, H. Ma and A. K. Y. Jen, *Adv. Mater.*, 2012, **24**, 828–833; (*c*) R. J. Tseng, J. X. Huang, J. Ouyang, R. B. Kaner and Y. Yang, *Nano Lett.*, 2005, **5**, 1077–1080; (*d*) C. X. Wu, F. S. Li, T. L. Guo and T. W. Kim, *Org. Electron.*, 2012, **13**, 178–183.

9 (*a*) X. D. Zhuang, Y. Chen, G. Liu, P. P. Li, C. X. Zhu, E. T. Kang, K. G. Noeh, B. Zhang, J. H. Zhu and Y. X. Li, *Adv. Mater.*, 2010, **22**, 1731–1735; (*b*) X. D. Zhuang, Y. Chen, B. X. Li, D. G. Ma, B. Zhang and Y. Li, *Chem. Mater.*, 2010, **22**, 4455–4461; (*c*) S. J. Liu, W. P. Lin, M. D. Yi, W. J. Xu, C. Tang, Q. Zhao, S. H. Ye, X. M. Liu and W. Huang, *J. Mater. Chem.*, 2012, **22**, 22964–22970; (*d*) S. Baek, D. Lee, J. Kim, S. H. Hong, O. Kim and M. Ree, *Adv. Funct. Mater.*, 2007, **17**, 2637–2644; (*e*) H. C. Wu, A. D. Yu, W. Y. Lee, C. L. Liu and W. C. Chen, *Chem. Commun.*, 2012, **48**, 9135–9137.

10 (*a*) B. Zhang, G. Liu, Y. Chen, C. Wang, K. G. Neoh, T. Bai and E. T. Kang, *ChemPlusChem*, 2012, **77**, 74–81; (*b*) S. J. Liu, P. Wang, Q. Zhao, H. Y. Yang, J. Wong, H. B. Sun, X. C. Dong, W. P. Lin and W. Huang, *Adv. Mater.*, 2012, **24**, 2901–2905; (*c*) S. G. Hahm, N. G. Kang, W. Kwon, K. Kim, Y. K. Ko, S. Ahn, B. G. Kang, T. Chang, J. S. Lee and M. Ree, *Adv. Mater.*, 2012, **24**, 1062–1066.

11 (*a*) T. Kurosawa, Y. C. Lai, T. Higashihara, M. Ueda, C. L. Liu and W. C. Chen, *Macromolecules*, 2012, **45**, 4556–4563; (*b*) F. Chen, G. Tian, L. Shi, S. Qi and D. Wu, *RSC Adv.*, 2012, **2**, 12879–12885; (*c*) Y. Liu, Y. Zhang, Q. Lan, S. Liu, Z. Qin, L. Chen, C. Zhao, Z. Chi, J. Xu and J. Economy, *Chem. Mater.*, 2012, **24**, 1212–1222; (*d*) S. G. Hahm, S. Choi, S. H. Hong, T. J. Lee, S. Park, D. M. Kim, W. S. Kwon, K. Kim, O. Kim and M. Ree, *Adv. Funct. Mater.*, 2008, **18**, 3276–3282; (*e*) Q. Liu, K. Jiang, Y. Wen, J. Wang, J. Luo and Y. Song, *Appl. Phys. Lett.*, 2010, **97**, 253304; (*f*) Y. Li, Y. Chu, R. Fang, S. Ding, Y. Wang, Y. Shen and A. Zheng, *Polymer*, 2012, **53**, 229–240.

12 (*a*) D. B. Velusamy, S. K. Hwang, R. H. Kim, G. Song, S. H. Cho, I. Bae and C. Park, *J. Mater. Chem.*, 2012, **22**, 25183–25189; (*b*) M. A. Khan, U. S. Bhansali, D. Cha and H. N. Alshareef, *Adv. Funct. Mater.*, 2013, **23**, 2145–2152; (*c*) S. Gao, C. Song, C. Chen, F. Zeng and F. Pan, *J. Phys. Chem. C*, 2012, **116**, 17955–17959; (*d*) C. J. Chen, Y. C. Hu and G. S. Liou, *Chem. Commun.*, 2013, **49**, 2804–2806; (*e*) L. Q. Xu, B. Zhang, K. G. Neoh, E. T. Kang and G. D. Fu, *Macromol. Rapid Commun.*, 2013, **34**, 234–238; (*f*)

M. A. Mamo, A. O. Sustaita, N. J. Coville and I. A. Hummelgen, *Org. Electron.*, 2013, **14**, 175–181.

13 (*a*) C. J. Chen, H. J. Yen, W. C. Chen and G. S. Liou, *J. Mater. Chem.*, 2012, **22**, 14085–14093; (*b*) T. J. Lee, C. W. Chang, S. G. Hahm, K. Kim, S. Park, D. M. Kim, J. Kim, W. S. Kwon, G. S. Liou and M. Ree, *Nanotechnology*, 2009, **20**, 135204; (*c*) K. Kim, H. J. Yen, Y. G. Ko, C. W. Chang, W. Kwon, G. S. Liou and M. Ree, *Polymer*, 2012, **53**, 4135–4144; (*d*) Y. G. Ko, W. Kwon, H. J. Yen, C. W. Chang, D. M. Kim, K. Kim, S. G. Hahm, T. J. Lee, G. S. Liou and M. Ree, *Macromolecules*, 2012, **45**, 3749–3758; (*e*) Y. L. Liu, K. L. Wang, G. S. Huang, C. X. Zhu, E. S. Tok, K. G. Neoh and E. T. Kang, *Chem. Mater.*, 2009, **21**, 3391–3399; (*f*) T. J. Lee, Y. G. Ko, H. J. Yen, K. Kim, D. M. Kim, W. Kwon, S. G. Hahm, G. S. Liou and M. Ree, *Polym. Chem.*, 2012, **3**, 1276–1283; (*g*) A. D. Yu, T. Kurosawa, Y. C. Lai, T. Higashihara, M. Ueda, C. L. Liu and W. C. Chen, *J. Mater. Chem.*, 2012, **22**, 20754–20763; (*h*) H. Y. Yen, C. J. Chen and G. S. Liou, *Adv. Funct. Mater.*, 2013, DOI: 10.1002/adfm.201300569.

14 (*a*) S. H. Cheng, S. H. Hsiao, T. X. Su and G. S. Liou, *Macromolecules*, 2005, **38**, 307–316; (*b*) G. S. Liou, S. H. Hsiao and T. X. Su, *J. Mater. Chem.*, 2005, **15**, 1812–1820; (*c*) G. S. Liou, Y. L. Yang and Y. L. Oliver Su, *J. Polym. Sci., Part A: Polym. Chem.*, 2006, **44**, 2587–2603; (*d*) G. S. Liou, S. H. Hsiao and H. W. Chen, *J. Mater. Chem.*, 2006, **16**, 1831–1842; (*e*) G. S. Liou, S. H. Hsiao, N. K. Huang and Y. L. Yang, *Macromolecules*, 2006, **39**, 5337–5346; (*f*) G. S. Liou, H. W. Chen and H. J. Yen, *J. Polym. Sci., Part A: Polym. Chem.*, 2006, **44**, 4108–4121; (*g*) G. S. Liou, H. W. Chen and H. J. Yen, *Macromol. Chem. Phys.*, 2006, **207**, 1589–1598; (*h*) G. S. Liou, C. W. Chang, H. M. Huang and S. H. Hsiao, *J. Polym. Sci., Part A: Polym. Chem.*, 2007, **45**, 2004–2014; (*i*) G. S. Liou, S. H. Hsiao, W. C. Chen and H. J. Yen, *Macromolecules*, 2006, **39**, 6036–6045; (*j*) G. S. Liou and H. J. Yen, *J. Polym. Sci., Part A: Polym. Chem.*, 2006, **44**, 6094–6102; (*k*) H. J. Yen and G. S. Liou, *J. Polym. Sci., Part A: Polym. Chem.*, 2009, **47**, 1584–1594; (*l*) H. J. Yen and G. S. Liou, *J. Mater. Chem.*, 2010, **20**, 9886–9894; (*m*) G. S. Liou and H. J. Yen, Polyimides, in *Polymer Science: A Comprehensive Reference*, ed. K. Matyjaszewski and M. Möller, 2012, vol. 5, pp. 497–535.

15 M. J. Frisch, G. W. Trucks, H. B. Schlegel, G. E. Scuseria, M. A. Robb, J. R. Cheeseman, G. Scalmani, V. Barone, B. Mennucci, G. A. Petersson, H. Nakatsuji, M. Caricato, X. Li, H. P. Hratchian, A. F. Izmaylov, J. Bloino, G. Zheng, J. L. Sonnenberg, M. Hada, M. Ehara, K. Toyota, R. Fukuda, J. Hasegawa, M. Ishida, T. Nakajima, Y. Honda, O. Kitao, H. Nakai, T. Vreven, J. A. Montgomery, Jr., J. E. Peralta, F. Ogliaro, M. Bearpark, J. J. Heyd, E. Brothers, K. N. Kudin, V. N. Staroverov, R. Kobayashi, J. Normand, K. Raghavachari, A. Rendell, J. C. Burant, S. S. Iyengar, J. Tomasi, M. Cossi, N. Rega, J. M. Millam, M. Klene, J. E. Knox, J. B. Cross, V. Bakken, C. Adamo, J. Jaramillo, R. Gomperts, R. E. Stratmann, O. Yazyev, A. J. Austin, R. Cammi, C. Pomelli, J. Ochterski, R. L. Martin, K. Morokuma, V. G. Zakrzewski, G. A. Voth, P. Salvador, J. J. Dannenberg, S. Dapprich, A. D. Daniels, O. Farkas, J. B. Foresman, J. V. Ortiz, J. Cioslowski and D. J. Fox, *Gaussian 09 (Revision D.01)*, Gaussian, Inc., Wallingford, CT, 2009.

16 (*a*) C. W. Chang, G. S. Liou and S. H. Hsiao, *J. Mater. Chem.*, 2007, **17**, 1007–1015; (*b*) G. S. Liou and C. W. Chang, *Macromolecules*, 2008, **41**, 1667–1674; (*c*) S. H. Hsiao, G. S. Liou, Y. C. Kung and H. J. Yen, *Macromolecules*, 2008, **41**, 2800–2808; (*d*) C. W. Chang, C. H. Chung and G. S. Liou, *Macromolecules*, 2008, **41**, 8441–8451; (*e*) C. W. Chang and G. S. Liou, *J. Mater. Chem.*, 2008, **18**, 5638–5646; (*f*) C. W. Chang, H. J. Yen, K. Y. Huang, J. M. Yeh and G. S. Liou, *J. Polym. Sci., Part A: Polym. Chem.*, 2008, **46**, 7937–7949; (*g*) H. J. Yen and G. S. Liou, *Org. Electron.*, 2010, **11**, 299–310; (*h*) L. T. Huang, H. J. Yen, C. W. Chang and G. S. Liou, *J. Polym. Sci., Part A: Polym. Chem.*, 2010, **48**, 4747–4757.

17 (*a*) G. S. Liou and H. Y. Lin, *Macromolecules*, 2009, **42**, 125–134; (*b*) M. Robin and P. Day, *Adv. Inorg. Chem. Radiochem.*, 1967, **10**, 247–422; (*c*) S. Mazur, P. S. Lugg and C. Yarnitzky, *J. Electrochem. Soc.*, 1987, **134**, 346–353.

